

# Glacier Moraine Formation-Mimicking Colloidal Particle Assembly in Microchanneled, Bioactive Hydrogel for Guided Vascular Network Construction

Min Kyung Lee, Max H. Rich, Artem Shkumatov, Jae Hyun Jeong, Marni D. Boppart, Rashid Bashir, Martha U. Gillette, Jonghwi Lee,\* and Hyunjoon Kong\*

Spatial organization of drug-releasing microparticles within cell adherent three-dimensional (3D) matrices has long been sought to direct cellular phenotypic activities involved in tissue morphogenesis, and, ultimately, improve the quality of tissue regeneration therapies. However, the lack of tools made it difficult to achieve this goal. This study resolves the challenge through the uniaxial freeze-drying of a microparticle-loaded hydrogel, which temporally increases the wall shear stress on the resulting microchannels in the 3D matrix. Subsequently, the shear stress

aligned the microparticles along the microchannel walls, similar to glacier-induced moraine formation. The encapsulation of vascular endothelial growth factor (VEGF) into these aligned microparticles stimulated vascular ingrowth into the microchanneled hydrogel more significantly than a conventional microporous hydrogel, in which microparticles were randomly distributed. When the hydrogel was implanted onto ischemic muscle, it greatly served to enhance perfusion recovery of a murine ischemic hindlimb. Such an advanced hydrogel as was developed in this study would be useful to better understand and direct cellular emergent behavior towards regeneration of various tissues. This material assembly process would be also useful in tailoring the microstructure and properties of a wide array of hydrogel systems in a refined manner.

Over the last decades, vast efforts were made to assemble polymeric constructs enabling 3D cell culture and transplantation in order to study and further regulate diverse cellular phenotypic, physiological, and regenerative activities in an elaborate manner.<sup>[1–7]</sup> These cell-material systems were also modified to create functional tissues similar to native ones that can be used in various applications including clinical treatments of tissue defects and assembly of intelligent living machinery.<sup>[8–10]</sup> One popular approach in these efforts is to load microparticles capable of sustainably releasing bioactive molecules (e.g., growth factors and cytokines) in various microporous materials devised to stimulate cell migration and adhesion.<sup>[11,12]</sup> However, most assembly methods encountered had a limited capability to control the spatial distribution of microparticles releasing bioactive molecules. Consequently, it is difficult to stimulate cellular activities critical to generate desired forms of functional tissues of interests in a 3D matrix. These drawbacks signify the need to develop a simple, advanced method to fabricate materials in which bioactive microparticles are presented in a predefined 3D micropattern.

In this study, we hypothesized that sequential uniaxial freeze-drying and rehydration of a hydrogel loaded with microparticles would create a microchanneled gel construct in which microparticles were aligned with the microchannel direction in situ. Similar to the natural process to form a moraine on the river-side during glacier formation, such microparticle organization may be caused by unilateral ice column growth that increases freezing-induced shear stress on the resulting stationary gel-forming polymeric layer (**Figure 1a**). The remodeled gel would stimulate vascular growth through the microchannels aligned with VEGF-releasing microparticles and further enhance

Dr. M. K. Lee, M. H. Rich, Prof. H. J. Kong  
Department of Chemical  
and Biomolecular Engineering  
Institute of Genomic Biology  
University of Illinois at Urbana-Champaign  
Urbana, IL 61801, USA



A. Shkumatov  
Department of Pathobiology  
University at Illinois at Urbana-Champaign  
Urbana, IL 61801, USA  
E-mail: hjkong06@illinois.edu

Prof. J. H. Jeong  
Department of Chemical Engineering  
Soongsil University  
Seoul 156–743, Korea

Prof. M. D. Boppart  
Department of Kinesiology and Community Health  
University of Illinois at Urbana-Champaign  
IL 61801, USA

Prof. M. D. Boppart  
Beckman Institute for Advanced Science  
and Technology  
University of Illinois at Urbana-Champaign  
IL 61801, USA

Prof. R. Bashir  
Department of Electrical and Computer Engineering & Bioengineering  
University of Illinois at Urbana-Champaign  
IL 61801, USA

M. U. Gillette  
Neuroscience Program  
Department of Cell and Developmental Biology  
University of Illinois at Urbana-Champaign  
IL 61801, USA

Prof. J. Lee  
Department of Chemical Engineering and Materials Science  
Chung-Ang University  
Seoul 156–756, Korea  
jong@cau.ac.kr

DOI: 10.1002/adhm.201400153

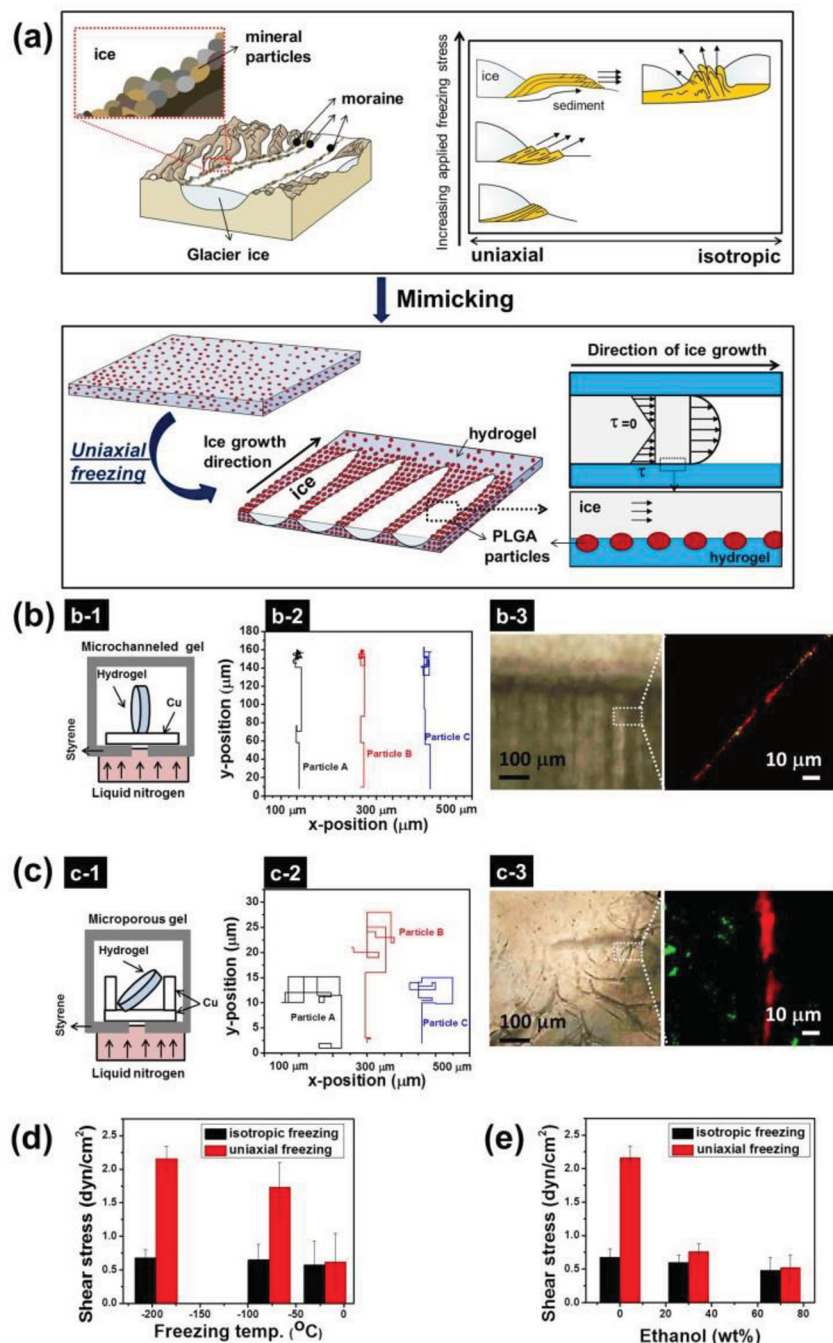


**Figure 1.** a) Schematic describing the uniaxial freeze-drying process used to align PLGA microparticles in microchannels of a hydrogel, similar to the process of glacier formation on the riverside. During the glacier formation, minerals suspended in water are sheared and stacked on a riverside due to increased shear stress. The resulting hydrogel was used to control the growth direction and spacing of vascular and neural networks. b) Effects of uniaxial freezing on hydrogel remodeling and microparticle organization. b-1) A schematic describing the experimental set-up for uniaxial freezing of the alginate hydrogel loaded with PLGA microparticles. b-2) Analysis of PLGA particle displacements during uniaxial freezing. b-3) A snapshot of uniaxial ice column-growth during uniaxial freezing of the hydrogel (left images). The unilateral ice column growth resulted in the co-localization of PLGA microparticles (green) and alginate layer (red), as displayed in the right, fluorescent image. c) Effects of isotropic freezing on hydrogel remodeling and microparticle organization. c-1) A schematic describing an experimental set-up for isotropic freezing of the alginate hydrogel loaded with PLGA microparticles. c-2) Analysis of PLGA particle displacement during isotropic freezing. In b-2) and c-2), displacements of three separate particles were presented among 30 particles analyzed. c-3) A snapshot of isotropic growth of ice columns during isotropic freezing (left image), which led to arbitrary distribution of PLGA microparticles (green), separately from alginate (red), as displayed in the right, fluorescent image. d) Effects of freezing temperature on freezing-induced shear stress of the alginate layer formed during freezing process. e) Effects of ethanol fraction in aqueous media used to prepare the pre-gel solution on freezing-induced shear stress of the alginate layer formed during freezing process. The shear stress values were calculated from displacements of PLGA microparticles during freezing. Values and error bars in d) and e) represent average and standard deviation of the displacements of 6 particles.

treatments of an ischemic muscle resulting from vascular ligation. We examined this hypothesis by using alginate coupled with cell adhesion peptides<sup>[13]</sup> as a model gel-forming polymer and poly(lactide-co-glycolic acid) (PLGA) microparticles as a model VEGF-encapsulating microparticles.<sup>[11]</sup> The capabilities of the material to control spatial organization of endothelial cells (ECs) and subsequent growth direction of blood vessel were evaluated by examining cell migration into the gel in vitro and also vascularization of the gel implanted on a chicken chorioallantoic membrane. We also implanted the microchanneled hydrogel in a murine ischemic hindlimb to assess the capability of the gel to improve perfusion recovery via neovascularization.<sup>[14]</sup>

First, we examined whether the freezing direction of a hydrogel would control spatial organization of PLGA microparticles in the gel matrix. The hydrogel loaded with PLGA microparticles was prepared by adding adipic acid dihydrazide, a cross-linker, into an aqueous mixture of PLGA microparticles and alginate. Subsequently, the gel was placed on a copper plate cooled by liquid nitrogen at  $-196\text{ }^{\circ}\text{C}$  (Figure 1b-1). Instantaneously, ice columns with an average diameter of  $100\text{ }\mu\text{m}$  uniaxially grew through the gel matrix (Figure S1a-1, Supporting Information). The advancing rate of ice columns, quantified with real-time microscopic imaging (Video S1a, Supporting Information), was approximately  $25\text{ }\mu\text{m s}^{-1}$ . All ice columns were aligned perpendicular to the copper surface. A thin alginate layer surrounded individual ice column. The cross-sectional density of ice column was approximately  $2.5 \times 10^3\text{ cm}^{-2}$ .

During the uniaxial freezing process, PLGA microparticles randomly suspended in the gel vertically moved along the direction of ice growth, approximately  $160\text{ }\mu\text{m}$  upwards, as monitored with fluorescently labeled microparticles (Figure 1b-3). A mean square displacement of microparticles,  $\langle d^2 \rangle_{\text{PLGA}}$ , was

approximately  $800 \mu\text{m}^2$  (Figure 1b-2). The displacement coefficient of PLGA microparticle ( $D_{\text{PLGA}}$ ), calculated from  $\langle d^2 \rangle_{\text{PLGA}}$  using Equation (1)

$$D(\Delta t) = \frac{\langle d^2 \rangle}{4\Delta t} \quad (1)$$

where  $\Delta t$ , the freezing time, was approximately  $185 \mu\text{m}^2 \text{s}^{-1}$ . Throughout this process, microparticles were separated from ice columns and localized in the cross-linked alginate layer, as confirmed with co-localization of fluorescein-labeled microspheres and rhodamine-labeled alginate (Figure 1b-3).

In contrast, an alginate gel placed in a copper container at  $-196 \text{ }^\circ\text{C}$  displayed isotropic ice growth (Figure 1c-1). Accordingly, cross-linked alginate of a gel matrix was reorganized without any defined directionality (Figure S1a-2, Supporting Information). During the matrix remodeling, PLGA microparticles in the gel were minimally displaced (Figure 1c-2 and Video S1b, Supporting Information). The  $\langle d^2 \rangle_{\text{PLGA}}$  measured using fluorescein-labeled microparticles was approximately  $200 \mu\text{m}^2$ , which was fourfold smaller than that resulting from the uniaxial freezing process. As such, particles were kept randomly distributed in a frozen gel construct, without being co-localized with the cross-linked alginate layer (Figure 1c-3, Supporting Information).

We further analyzed whether such freezing-induced particle rearrangement was related to shear stress exerted on the remodeled alginate layer. The advancing rate of the ice column ( $Q_{\text{ice}}$ ), quantified with a real-time imaging, was one-order magnitude larger with the uniaxial freezing process than the isotropic freezing process (Table S1, Supporting Information). The freezing-induced shear stress ( $\tau$ ) on the alginate layer, calculated from  $Q_{\text{ice}}$  using<sup>[15]</sup>

$$\tau = \eta \frac{6Q}{WH^2} \quad (2)$$

where  $W$  is the gel width (5 mm),  $H$  is the gel height (0.5 mm), and  $\eta$  is the water viscosity (1 mPa S), was approximately three times larger during the uniaxial freezing process (Table S1, Supporting Information). Accordingly, the freezing-induced shear stress, calculated by multiplying the shear stress with water viscosity, was  $2.2 \text{ dyne cm}^{-2}$ , which was three times larger than that resulting from the isotropic freezing process.

Such stress-induced particle assembly was negated by the copper plate temperature and solvent composition. Increasing temperature of the copper plate on which the gel was placed from  $-196$  to  $-20 \text{ }^\circ\text{C}$  abolished uniaxial ice growth and subsequent anisotropic alignment of PLGA microparticles. According to calculation, the freezing-induced shear stress significantly decreased from  $1.7$  to  $0.6 \text{ dyne cm}^{-2}$  with increasing freezing temperature. The shear stress obtained at  $-20 \text{ }^\circ\text{C}$  was rather comparable to that attained by isotropic freezing (Figure 1d). In addition, increasing mass fraction of ethanol from 30% to 70% also failed to reorganize microparticles (Figure S1b, Supporting Information). Incorporation of ethanol in media significantly decreased the freezing-induced shear stress to  $0.5 \text{ dyne cm}^{-2}$ , which is also comparable to the freezing-induced shear stress during the isotropic freezing process (Figure 1e).

Next, the uniaxially frozen hydrogels were lyophilized to introduce microchannels with anisotropic alignment. According to micro-CT images, this process generated microchannels with an average diameter of  $100 (\pm 15) \mu\text{m}$ . The microchannels were anisotropically aligned to each other (Figure 2a-1 and Video S2a, Supporting Information). In addition, according to scanning electron microscopic (SEM) images, PLGA microparticles were aligned with the microchannel, while being partially embedded in the channel wall (Figure 2a-2 and Figure 2a-3). The average spacing of these particles was approximately  $20 (\pm 5) \mu\text{m}$ . In contrast, lyophilization of hydrogels with isotropically oriented ice columns created micropores with inhomogeneous diameter and poor interconnectivity (Figure 2b-1, and Video S2b, Supporting Information). In addition, microparticles were mostly separated from the dehydrated matrix (Figure 2b-2, Figure 2b-3, and Figure S1c, Supporting Information).

Finally, these lyophilized matrices were rehydrated to form microchanneled or microporous hydrogels. The different rehydration behaviors of microchanneled and microporous gels were confirmed with colored media (Figure S2a,b, Supporting Information). Water was more uniformly distributed in, and also more strongly bound to the microchanneled gel than that added into the microporous gel, according to magnetic resonance imaging (MRI) (Figure 2c). The degree of swelling for the microchanneled gel was also 1.3-fold higher than the microporous gel (Figure S2c, Supporting Information). In the microchanneled gel, PLGA microparticles were kept localized in microchannel walls during incubation in phosphate buffer saline (PBS) over 7 d, while the microporous gel lost significant number of PLGA microparticles (Figure S3, Supporting Information).

The bulk elastic modulus of the microchanneled gel significantly depended on the direction of external force (Figure 2d). The elastic modulus of the hydrogel compressed along the microchannel direction ( $E_{\parallel}$ ) was almost ninefold higher than that of the gel compressed perpendicular to the microchannel direction, termed ( $E_{\perp}$ ).  $E_{\parallel}$  was comparable to  $E$  of the original gel before freeze-drying. In addition,  $E_{\parallel}$  of the microchanneled gel was 10-fold larger than  $E$  of the microporous gel.

Using the hydrogels assembled through uniaxial freeze-drying and rehydration process, we examined whether the microchannel and microparticles in a matrix orchestrate to stimulate angiogenesis, characterized with endothelial sprouting from preexisting blood vessels<sup>[16]</sup> (Figure S4, Supporting Information). The VEGF was loaded into PLGA microparticles, so the VEGF released from the microparticles would stimulate migration and endothelial lumen formation within the gel matrix. The gel matrix was also prepared with alginate conjugated with integrin-binding oligopeptides containing Arg-Gly-Asp sequence,<sup>[17]</sup> termed RGD-alginate, in order to facilitate cellular migration into microchannels or micropores of the gel matrix. According to the analysis of VEGF amount released from a hydrogel, the microchanneled gel released more VEGF than the microporous gel, because of the higher level of particle retention and larger permeability (Figure S5, Supporting Information).

The resulting hydrogels were embedded in collagen gels laden with endothelial cells (ECs), in order to examine migration of ECs into the gel and subsequent endothelial lumen

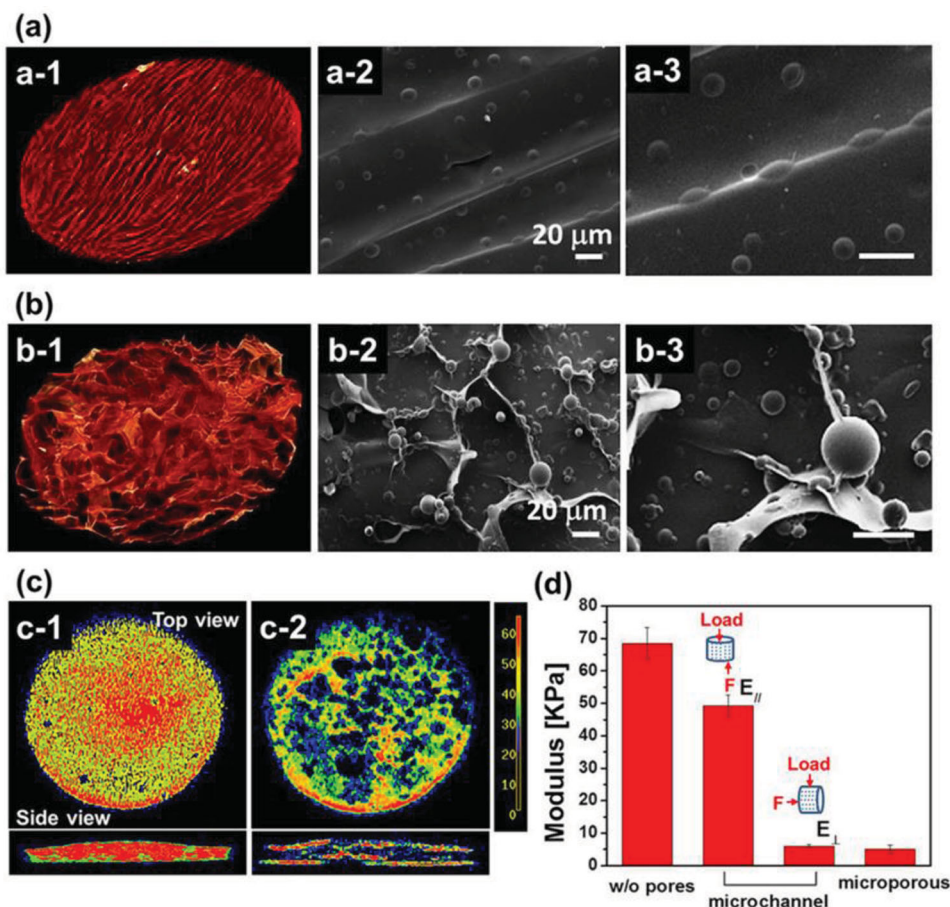


**Figure 2.** Microstructural characterization of PLGA microparticle-loaded alginate gel remodeled via freeze-drying process. a) Micro-CT 3D image (a-1) and SEM images (a-2, a-3) of the microchanneled, alginate matrix loaded with PLGA microparticles. The microchanneled matrix was prepared by sequential uniaxial freezing and lyophilization of the alginate hydrogel. Image (a-3) is a magnified view of the PLGA microparticles partially embedded in uniaxial, microchannels of the alginate matrix. b) Micro-CT 3D image (b-1) and SEM images (b-2, b-3) of the microporous, alginate matrix loaded with PLGA microparticles. The microporous matrix was prepared by sequential isotropic freezing and lyophilization of the alginate hydrogel. Image (b-3) is a magnified view of the PLGA microparticles separated from the microporous alginate matrix. c) MR images to show water distribution in rehydrated, microchanneled alginate hydrogel (c-1) and microporous alginate hydrogel (c-2). The freeze-dried alginate matrix was rehydrated with deionized water or PBS. d) The compressive elastic moduli of the alginate hydrogel prior to freeze drying (w/o pores), the microchanneled, hydrogel compressed in parallel with microchannel direction ( $E_{||}$ ), the microchanneled, hydrogel compressed, perpendicular to microchannel direction ( $E_{\perp}$ ), and microporous hydrogel.

formation (Figure S6, Supporting Information). Interestingly, ECs actively migrated into microchannels of the hydrogel, whereas few cells migrated into the microporous gel. Subsequently, a larger number of endothelial lumens were formed within microchannels (Figure 3a-1, and Figure S6a, Supporting Information). The average spacing of endothelial lumen was about  $102 (\pm 11) \mu\text{m}$ , equivalent to the spacing of microchannels. Cells that constitute the endothelial lumen displayed highly stretched actin filaments, which implicated active cell-cell junction. The hydrogel free of VEGF-releasing PLGA microparticles or RGD peptides did not stimulate cellular migration into microchannels. Besides, very few ECs migrated into the microporous hydrogel (Figure 3b-1, and Figure S6b, Supporting Information).

The microchanneled, VEGF-releasing RGD-alginate hydrogel also facilitated vascular growth into the gel, when it was implanted on chicken chorioallantoic membrane (CAMs) (Figure S4,

Supporting Information, and Figure 3a-2). Similar to in vitro studies, fewer blood vessels grew into the microporous gel (Figure 3b-2). According to cross-sectional, histological images of the gel implants, the number of mature blood vessels positively stained for  $\alpha$ -smooth muscle actin was threefold larger with the microchanneled gel than the microporous gel (Figure 3a-3, Figure 3b-3, and Figure S7, Supporting Information).

Also, the microchanneled, VEGF-releasing RGD-alginate hydrogel implanted in an ischemic hindlimb greatly enhanced the perfusion recovery level (Figure 3c and Figure S8a, Supporting Information). The perfusion ratio, quantified with the Laser Doppler perfusion images<sup>[16]</sup> of ischemic hindlimb and intact one, reached 0.8 within 49 d. In contrast, the microporous, VEGF-releasing RGD-alginate gel increased the reperfusion ratio to 0.3, similar to the microchanneled, RGD-alginate hydrogel free of VEGF-releasing PLGA microparticles (Figure 3d). Such enhanced perfusion recovery was related

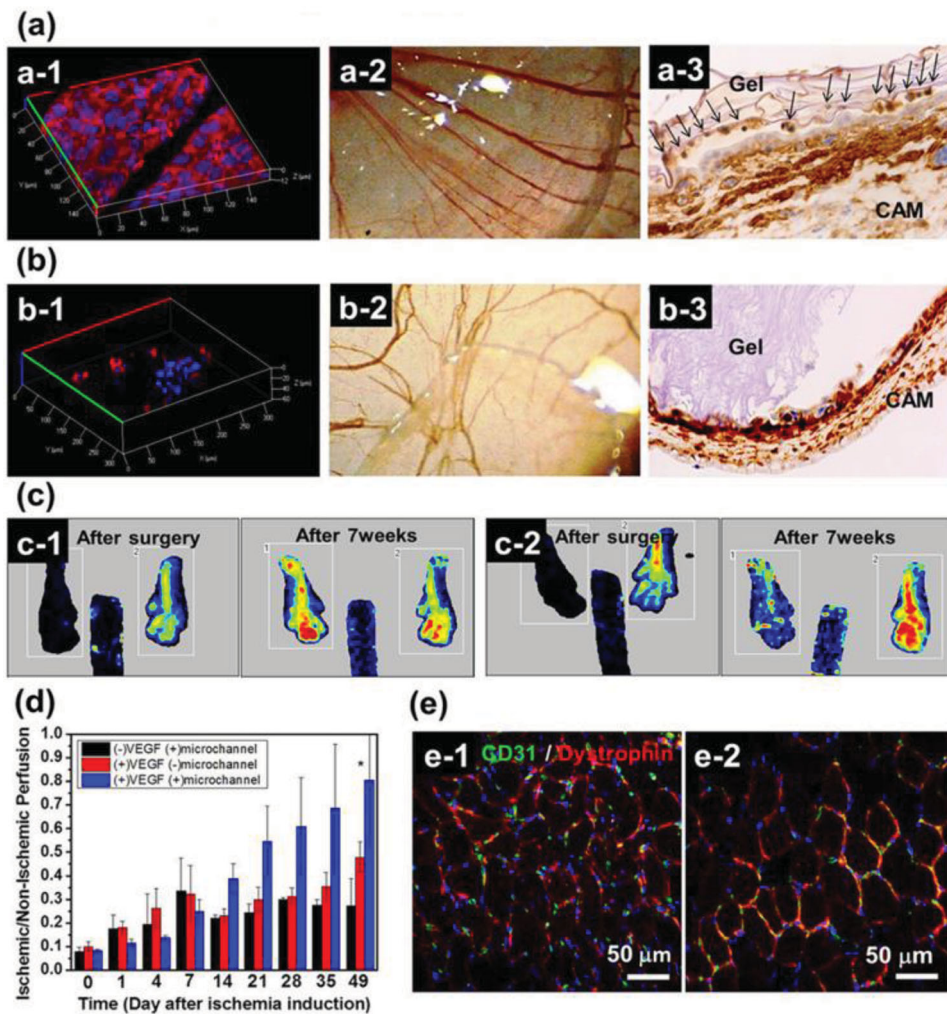


**Figure 3.** Regeneration of blood vessels and treatment of ischemic tissue using RGD-alginate hydrogels in which VEGF-releasing PLGA microparticles are aligned with microchannels. a,b-1) 3D z-stack images of endothelial cells that migrated into the microchanneled gel and formed endothelial lumen-like tubes (a-1) and those that underwent limited migration into the microporous gel (b-1). a,b-2) Optical top-view images of vascular networks formed through and around hydrogels implanted on CAM. The microchanneled hydrogel stimulated growth of straight blood vessels through microchannels (a-2), while the microporous hydrogel created randomly oriented vascular networks (b-2). a,b-2) a,b-3) Images of histological cross-sections of CAMs that were stained with the marker for  $\alpha$ -smooth muscle actin. Cross-section of the microchanneled gel displayed multiple, blood vessels with regular spacing, specifically in the area closer to the CAM (a-3). In contrast, cross-section of the microporous gel exhibited limited vascular growth into the implant (b-3). c) LDPI images of the ischemic, mouse feet treated with the microchanneled hydrogel (c-1) and the microporous hydrogel (c-2). The femoral artery of the left hindlimb was ligated to induce ischemia. The increase of perfusion ratio, quantified with the LDPI image, was most significant with a mouse implanted with the microchanneled hydrogel (d). The values between conditions, characterized on Day 49, were statistically significant ( $*p < 0.05$ ). e) Immunohistological, fluorescent images of cross-sections of skeletal muscle implanted with the microchanneled hydrogel (e-1) and microporous hydrogel (e-2). Blood vessels were stained with an antibody to CD31 and muscle was stained with an antibody to dystrophin. FITC(green) = CD31; rhodamine(red) = dystrophin.

to the significant increase of vascular density (Figure 3e). According to the analysis of the density of CD31-positive blood vessels in the hindlimb, the microchanneled VEGF-releasing RGD-alginate gel led to a 1.6-times greater increase of the capillary density than the microporous hydrogel system in which microparticles were randomly distributed (Figure 3e, and Figure S8b, Supporting Information). The ratio of blood vessel to muscle fiber was also 1.4-times higher with the microchanneled hydrogel system than the microporous gel (Figure S8c, Supporting Information).

Overall, our results successfully demonstrate that growth factor-releasing microparticles can be spatially organized in a microchanneled hydrogel by harnessing shear stress temporally increased during in situ uniaxial freezing. The resulting hydrogel could sequester microparticles in the microchannel walls more effectively than the hydrogel in which micropores were randomly connected. Further functionalization of microchannel walls with cell adhesion peptides stimulated endothelial lumen formation and neovascularization through microchannels. Implantation of the hydrogel in the ischemic muscle

therefore resulted in significantly enhanced recovery of perfusion because of the increase of vascular density.

It is well known that external shear stress temporally aligns microparticles suspended in media.<sup>[18–20]</sup> In contrast, this is the first demonstration that the temporal increase of shear stress at an interface between the ice column and the cross-linked polymer layer can permanently align particles in a 3D gel matrix. We suggest that the underlying mechanism to reorganize micro-sized particles in a gel matrix is similar to that to localize macro-sized mineral particles alongside a glacier formed in a river.<sup>[21]</sup> Such a process was advantageous in holding microparticles in desired microchannel walls and releasing larger amount of growth factors of interests. In contrast, a traditional random directional freeze drying failed to create the force to organize microparticles, thus leading to separation of microparticles from the gel matrix and, eventually, a significant loss of microparticles from the matrix.

There was an increasing number of nonpassing microchannels upon increasing either hydrogel diameter or thickness, likely due to limited range of heat transfer with the current set-up for uniaxial freezing. This limitation in process scalability may be readily resolved by further advancing the set-up for freezing. Additionally, the size of microchannels can be controlled by various experimental conditions such as freezing temperature, freezing rate, polymer/solvent types, polymer concentration, and solvent composition. This process could be also readily extended to a wide array of hydrogels loaded with microparticles (results not shown).

More interestingly, the microchanneled hydrogel with an uniaxial microparticle alignment was capable of stimulating vascular growth into microchannels and further enhancing perfusion recovery in the ischemic tissue, compared with microporous hydrogel in which a smaller number of microparticles were randomly distributed. We propose that a larger amount of VEGF release stimulates migration of ECs towards the matrix. These cells should be further stimulated to migrate into microchannels and form a capillary-like endothelial lumen,<sup>[22]</sup> likely because VEGF concentration in the microchannel would be higher than that outside the gel matrix. Integrin-binding cell adhesion peptides immobilized on the microchannel wall should be another significant factor to support cellular migration and morphogenic activities in the microchannels.<sup>[23]</sup> It is suggested that such materials' capability to guide vascular growth in the area of interests greatly serve to increase vascular density and further enhance recovery of perfusion in the ischemic hindlimb. Certain studies previously reported that a cryogel loaded with proangiogenic growth factors can stimulate angiogenesis at an implantation site.<sup>[24–26]</sup> However, to the best of our knowledge, no attempts were made to align growth factor-releasing microparticles in the microchannels of a gel and stimulate neovascularization through a gel matrix.

Taken together, we propose that this study should be a major step forward for the control of the spatial organization of bioactive signals. The gel fabricated in this study can present diverse bioactive signals by encapsulating multiple growth factors of interest into microparticles of a wide array of biocompatible and biodegradable polymers. The spatial organization of these bioactive signals may be further controlled at smaller length scales by assembling a fresh hydrogel with a sophisticated 3D printing

unit, such as a stereolithographic assembly apparatus,<sup>[9,27]</sup> and subsequently, conducting the uniaxial freeze-drying process.<sup>[23–30]</sup> Finally, the resulting gel construct will greatly serve to improve the understanding and quality of clinical treatments for various diseases and tissue defects through a better understanding of function, changes in phenotypic activity, and emergent behavior<sup>[31]</sup> in a wide variety of cells.

## Experimental Section

**Particle Assembly in Microchanneled Alginate Hydrogel:** Alginate ( $M_w \approx 250\,000\text{ g mol}^{-1}$ , FMC Biopolymer) or RGD-alginate sterilized via filtration was dissolved in 0.1 M 2-(N-morpholino)ethanesulfonic acid (MES) buffer at a concentration of 2% (w/v). The alginate solution was sequentially mixed with PLGA microparticles, sulfonated *N*-hydroxysuccinimide (Sulfo-NHS; Thermo Scientific), adipic acid dihydrazide (AAD; Sigma-Aldrich), and 1-ethyl-3-(3-dimethylaminopropyl)carbodiimide (EDC; Thermo Scientific). PLGA microparticles were encapsulated with VEGF via *in situ* double emulsification. The pregelled mixture was cured in a space between two glass plates separated by 1 mm spacer. Then, hydrogel disks with 5-mm diameter were punched out, and incubated in DI water at room temperature for 12 h. Then, to prepare the microchanneled hydrogel, the gel disk was placed on top of a copper plate with controlled temperatures. All gels were surrounded by styrene foam for insulation. The frozen sample was freeze-dried to introduce microchannels through the alginate gel disk. Finally, the dehydrated, microchanneled matrix was rehydrated by dropping aqueous media or cell suspension on the top of the sample. In contrast, the microporous gel was prepared via sequential freezing of the alginate gel in a copper container, lyophilization, and rehydration. The resulting PLGA particle arrangement in the microchannels or micropores of the gel was examined using an optical microscope, SEM, and micro-CT. Mechanical stiffness of the gel was evaluated by measuring an elastic modulus. The interaction between water and gel was evaluated with MRI.

**Microfabrication of the Microchanneled Hydrogel Constituted with Unmodified Alginate Gel Blocks and RGD-Alginate Gel Blocks:** The unmodified alginate gel strips with 500  $\mu\text{m}$  spacing were prepared by activating carbodiimide-modulated cross-linking reaction between alginate and AAD under a poly(dimethoxysiloxane) stamp with a predefined positive pattern. Subsequently, the space between the unmodified alginate gels was filled with the RGD-alginate solution to form the RGD-alginate gel. The resulting hydrogel was placed on a copper plate with temperature of  $-196\text{ }^\circ\text{C}$  to induce ice column growth through the gel. Then, the frozen gel was lyophilized to introduce microchannels in both unmodified alginate and RGD-alginate gel blocks. Finally, when needed, the dehydrated matrix was rehydrated with aqueous media, or cell suspension.

**In Vitro Cell Studies:** The gel's ability to stimulate migration and endothelial lumen formation of ECs was evaluated by embedding the gel of interests into a collagen gel dispersed with ECs at a density of  $5 \times 10^6\text{ cells mL}^{-1}$ . Cells adhered to microchannels or micropores of the gel were studied by staining their actin filaments and nuclei with fluorescent phalloidin and DAPI, respectively, and imaging them with laser scanning confocal microscope (Leica, LSM700).

**In Vivo Chick Chorioallantoic Membrane-Based Angiogenesis Assay:** *In vivo* angiogenesis assay was performed by implanting gels on the chick chorioallantoic membranes (CAMs) of one week old, fertilized chicken embryos. After one week of incubation at  $37\text{ }^\circ\text{C}$ , CAMs were excised at the implantation area and samples were embedded in paraffin, sectioned, and stained with an antibody to  $\alpha$ -smooth muscle actin ( $\alpha$ -SMA). The CAM cross-sections were analyzed for mature blood vessel density using Image J. For each condition, four to six samples were implanted and evaluated.

**Ischemic Hindlimb Treatment:** The surgery to induce hindlimb ischemia was performed in accordance with the protocol approved by the Illinois

Institutional Animal Care and Use Committee. The microchanneled hydrogel and two control groups were implanted into the ischemic hindlimb of C57BL/6 mice (Jackson Laboratory). The overall impact of vascular growth on hindlimb perfusion was monitored by Laser Doppler Perfusion Imaging (LDPI) of the feet. Scans were taken of the ischemic and nonischemic limbs. The hindlimb tissue was dissected and stained with antibodies to CD31 and dystrophin, and fluorescent secondary antibodies. The immunostained tissues were imaged using the confocal microscope (LSM700, Zeiss).

**Statistical Analysis:** All averaged data are presented as means  $\pm$  SE. To determine significance, comparisons between groups were performed by one-way ANOVA followed by Tukey's Multiple Comparison Test ( $p < 0.05$ ).

## Supporting Information

Supporting Information is available from the Wiley Online Library or from the author.

## Acknowledgements

This work was supported by National Science Foundation (CAREER: DMR-0847253 to H.K., STC-EBICS Grant CBET-0939511 to H.K. and R.B.), US Army Telemedicine and Advanced Technology Research Center (W81XWH-08-1-0701 to H.K. and R.B.), UIUC-IGB Proof of Concept Award (to H.K. and R.B.), and National Research Foundation grant funded by the Korean Ministry of Science, ICT and Future Planning (NRF-2012R1A2A2A01014107 and NRF-2013R1A1A2021573 to J.L.). The authors wish to thank Mr. Frank Rauh (FMC BioPolymer) for the supply of alginate.

Received: March 18, 2014

Revised: April 26, 2014

Published online:

- [1] D. E. Discher, D. J. Mooney, P. W. Zandstra, *Science* **2009**, 324, 1673.
- [2] J. G. Gershovich, R. L. Dahlin, F. K. Kasper, A. G. Mikos, *Tissue Eng. Part A* **2013**, 19, 2565.
- [3] G. Eng, B. W. Lee, H. Parsa, C. D. Chin, J. Schneider, G. Linkov, S. K. Sia, G. Vunjak-Novakovic, *Proc. Natl. Acad. Sci.* **2013**, 110, 4551.
- [4] S. Zhang, *Nat. Biotechnol.* **2003**, 21, 1171.
- [5] Y. Luo, M. S. Shoichet, *Nat. Mater.* **2004**, 3, 249.
- [6] Y. Yang, K. Kulangara, J. Sia, L. Wang, K. W. Leong, *Lab Chip* **2011**, 11, 1638.
- [7] B. J. Lawrence, S. V. Madhally, *Cell Adh. Migr.* **2008**, 2, 9.
- [8] R. Langer, D. A. Tirrell, *Nat. Mater.* **2004**, 428, 487.
- [9] V. Chan, K. Park, M. B. Collens, H. Kong, T. A. Saif, R. Bashir, *Sci. Rep.* **2012**, 2, 857.
- [10] I. C. Kwon, Y. H. Bae, S. W. Kim, *Nature* **1991**, 354, 291.
- [11] F. R. Formiga, B. Pelacho, E. Garbayo, G. Abizanda, T. Simon-Yarza, M. Mazo, E. Tamayo, C. Jauquicoa, C. Ortiz-de-Solorzano, F. Prósper, M. J. Blanco-Prieto, *J. Controlled Release* **2010**, 147, 30.
- [12] K. Lee, E. A. Silva, D. J. Mooney, *J. R. Soc. Interface* **2011**, 8, 153.
- [13] S. E. D'Souza, M. H. Ginsberg, E. F. Plow, *Trends Biochem. Sci.* **1991**, 16, 246.
- [14] A. Limbourg, T. Korff, L. C. Napp, W. Schaper, H. Drexler, F. P. Limbourg, *Nat. Protocols* **2009**, 4, 1737.
- [15] G. R. Strobl, *The Physics of Polymers*, Springer, Berlin **1996**.
- [16] J. H. Jeong, V. Chan, C. Cha, P. Zorlutuna, C. Dyck, K. J. Hsia, R. Bashir, H. Kong, *Adv. Mater.* **2012**, 24, 58.
- [17] J. A. Rowley, D. J. Mooney, *J. Biomed. Mat. Res.* **2002**, 60, 217.
- [18] J. Michele, R. Patzold, R. Donis, *Rheol. Acta* **1977**, 16, 317.
- [19] M. K. Lyon, D. W. Mead, R. E. Elliott, L. G. Leal, *J. Rheol.* **2001**, 45, 881.
- [20] A. Y. Malkin, A. V. Semakov, V. G. Kulichikhin, *Adv. Colloid. Interface Sci.* **2010**, 157, 75.
- [21] P. Möller, *Quaternary Sci. Rev.* **2006**, 25, 362.
- [22] L. Laurent, L. B. Fabrice, H. Jacques, *Circ. Res.* **2007**, 100, 782.
- [23] R. Haubner, H. J. Wester, F. Burkhart, R. Senekowitsch-Schmidkte, W. Weber, S. L. Goodman, M. Schwaiger, *J. Nucl. Med.* **2001**, 42, 326.
- [24] M. Matsui, Y. Tabata, *Acta Biomater.* **2012**, 8, 1792.
- [25] G. Sun, X. Zhang, Y.-I. Shen, R. Sebastian, L. E. Dickinson, K. Fox-Talbot, M. Reinblatt, C. Steenbergen, J. W. Harmon, S. Gerecht, *Proc. Natl. Acad. Sci. U.S.A.* **2011**, 108, 20976.
- [26] S. A. Bencherif, R. W. Sands, D. Bhatta, P. Arany, C. S. Verbeke, D. A. Edwards, D. J. Mooney, *Proc. Natl. Acad. Sci. U.S.A.* **2012**, 109, 19590.
- [27] S. M. Peltola, F. P. Melchels, D. W. Grijpma, M. Kellomäki *Ann. Med.* **2008**, 40, 268.
- [28] S. Deville, E. Saiz, A. P. Tomsia, *Biomaterials* **2006**, 27, 5480.
- [29] H. Zhang, I. Hussain, M. Brust, M. F. Butler, S. P. Rannard, A. I. Cooper, *Nat. Mater.* **2005**, 4, 787.
- [30] M. K. Lee, N.-O. Chung, J. Lee, *Polymer* **2010**, 51, 6258.
- [31] J. R. Karr, J. C. Sanghvi, D. N. Macklin, M. V. Gutschow, J. M. Jacobs, B. Bolival, N. Assad-Garcia, J. I. Glass, M. W. Covert, *Cell* **2012**, 150, 389.